A role of villin-dependent F-actin organization in peroxisome motility in Arabidopsis cells

Calvin H. Huang [a], Amanda Koenig [b], Yuh-Ru Julie Lee [a], Yibo Shi [a], Jianping Hu [b,c,1], Bo Liu [a,1]

[a] Department of Plant Biology, College of Biological Sciences, University of California, Davis, CA 95616, U.S.A.

[b] Michigan State University-Department of Energy Plant Research Laboratory, Michigan State University, East Lansing, MI 48824, U.S.A.

[c] Department of Plant Biology, Michigan State University, East Lansing, MI 48824, U.S.A.

[1] Corresponding authors: Bo Liu, bliu@ucdavis.edu; Jianping Hu, huji@msu.edu

Short title: Villins and peroxisome motility

ABSTRACT

Actin microfilaments (F-actin) serve as the track for directional movement of organelles in plant cells. In actively growing plant cells, F-actin often form robust bundles that trespass the cellular dimension. To test how the F-actin network was employed for peroxisome movement, we wished to disturb actin organization by genetically compromising the function of villin (VLN) proteins that serve as the primary bundling factor in *Arabidopsis thaliana* cells. To do so, we isolated T-DNA insertional mutants in three *VLN* genes that were most actively expressed in vegetative tissues. We found that the *vln4* mutation greatly enhanced the growth defects caused by the *vln2 vln3* double mutant as the *vln2 vln3 vln4* triple mutant had a great reduction of organ growth and formed heavily deformed tissues. Both VLN2 and VLN4 proteins were detected on bundled F-actin filaments. Compared to the wild-type cells, the double and triple mutants exhibited progressively reduction of stable F-actin bundles and had fine F-actin filaments undergo rapid remodeling. The defective F-actin network did not prevent peroxisomes from taking on both rapid and slow movements along the F-actin tracks. However, we found that compromised F-actin bundling caused significant reductions in the speed of peroxisome movement and the displacement distance of peroxisome positions. Using a correlation analysis method, we also demonstrated that the complex heterogeneous peroxisome movement may be classified into clusters reflecting the directionality of peroxisome movement. The triple mutant suffered from a significant reduction of peroxisomes exhibiting long-range and linear movement. Our results provided insights into how VLN-dependent F-actin organization was coupled with the complex patterns of peroxisome movement.

INTRODUCTION

The single membrane organelle peroxisomes display rapid directional movement in the cytoplasm while exercising their essential functions of detoxification, β oxidation, and phytohormone synthesis. All these functions probably require peroxisome translocation throughout the cell to scavenge cytotoxins and coordinate with other cellular compartments for versatile metabolic reactions (Sandalio et al., 2021). In mammals, peroxisomes interact with the endoplasmic reticulum (ER), lipid droplets, lysozymes, and mitochondria during metabolic processes like fatty acid catabolism, and defects in peroxisomal distribution and inter-organellar interactions are the underlying cause of several diseases in humans (Wanders et al., 2023). In plants, peroxisomes also exhibit critical interactions with chloroplasts for detoxification, specialized metabolite synthesis, and photorespiration besides the interactions with the ER and mitochondria (Koenig et al., 2023; Pan et al., 2020). Additionally, peroxisomes participate in functions spanning subcellular topography, and their trafficking and spatial arrangement often are linked to the fluctuating demands of the cell during development or under stresses (He et al., 2021). The dynamic distribution of peroxisomes, therefore, requires agile motility along the cytoskeletal filaments and their associated motor proteins (Neuhaus et al., 2016).

In fungi and animals, peroxisome trafficking is primarily governed by microtubules and the associated motors of dynein and kinesins (Covill-Cooke et al., 2021; Salogiannis and Reck-Peterson, 2017). In plants, however, active movement of peroxisomes and other organelles predominately takes place on the F-actin tracks and is dependent on the motors in the Myosin XI subfamily (Avisar et al., 2008). In *Arabidopsis thaliana*, for example, actin depolymerization or inactivation of multiple Myosin XI genes causes nearly complete cessation of organelle movement (Mathur et al., 2002; Peremyslov et al., 2010). However, research to date has barely explored the molecular mechanisms that regulate actomyosin-dependent organelle movement in plants (Koenig et al., 2023). Typical differentiated plant cells have F-actin organized into two distinct populations of long and stable bundles and highly dynamic filaments (Henty-Ridilla et al., 2013). It is unclear whether organelles like peroxisomes employ either or both types of F-actin for their directional movement.

F-actin bundling in plants is primarily mediated by the villin (VLN) family proteins, which were initially isolated from lily pollen as abundant actin-binding proteins (Huang et al., 2015; Yokota et al., 2003). In Arabidopsis, VLN proteins encoded by five paralogous genes show various degrees of actin bundling capabilities both *in vitro* and *in vivo* (Li et al., 2025). Of the five

74 paralogs, *VLN2*, *VLN3* and *VLN4* are most broadly expressed in vegetative tissues. The *vln2*
75 *vln3* double mutants display a reduction in F-actin bundling and altered growth patterns with
76 twisted organs, but no significant compromise in vegetative growth (Bao et al., 2012; van der
77 Honing et al., 2012). Therefore, we hypothesized that VLN4 might function redundantly with
78 VLN2 and VLN3 in mediating organelle movement and the coupled growth processes in plants.
79 Here, we analyzed F-actin organization and peroxisome movement in the mutants of these
80 three Arabidopsis *VLN* genes that are highly expressed in vegetative tissues. Here we found
81 that the *vln2 vln3 vln4* triple mutant showed greatly reduced F-actin bundling and gross defects
82 in vegetative growth. The triple *vln* mutant allowed us to interrogate how compromised F-actin
83 bundling, without disassembling the entire F-actin network, impacted patterns of peroxisome
84 movement. Our results demonstrated that peroxisomes showed significantly reduced movement
85 speed and the displacement distance in the triple mutant. We also developed novel quantitative
86 methods to differentiate features associated with peroxisomal movement modes and correlate
87 such differences to the varied F-actin organization patterns.

88

89 **RESULTS**

90

91 **Deficient F-actin organization in the *vln* mutants**

92 Although peroxisomes are known to move along F-actin tracks by Myosin XI motors in plant
93 cells, it is unknown how the F-actin network is employed for the directional movement. We
94 sought to understand the role of actin organization, particularly F-actin bundling, in peroxisome
95 movement. Since the VLN proteins have been shown to contribute significantly to actin bundling
96 in plants (Huang et al., 2015), we aimed to employ the *vln* mutants in Arabidopsis to address the
97 potential role of F-actin bundling in peroxisome movement. Of the five Arabidopsis *VLN*
98 paralogs, *VLN2*, *VLN3* and *VLN4* are most broadly expressed in vegetative tissues according to
99 community-generated transcriptional data (https://bar.utoronto.ca/eplant/). It has recently been
100 reported that VLN2, VLN3, and VLN4 function redundantly in hypocotyl elongation, with VLN2
101 as the most abundant one in the hypocotyl, and that higher order *vln* mutants display aberrant
102 actin organization in their root and leaf cell (Li et al., 2025). Therefore, we predicted that these
103 three VLN proteins function redundantly to regulate organelle movement and the coupled
104 growth processes. To determine the role of VLN in peroxisome dynamics, we isolated the *vln4*
105 mutant and crossed it with the *vln2 vln3* (*vln2/3*) double mutant (Bao et al., 2012). As a result, a

106 *vln2 vln3 vln4* (*vln2/3/4*) triple mutant was independently generated, which displayed growth
107 defects (Suppl. Figure 1) similar to what was described recently (Li et al., 2025).

108 Because of the impact of actomyosin-dependent cell growth and the defect of shoot cell
109 elongation in the *vln2/3/4* mutant, we used hypocotyl cells to characterize the actin defects in
110 more detail before investigating peroxisomal dynamics in the mutants. We first confirmed that F-
111 actin cable formation is compromised in hypocotyl cells in both the double and triple *vln* mutants
112 by live-cell imaging of F-actin labeled by a LifeAct-GFP (green fluorescent protein) fusion
113 protein (Figure 1A). Compared to the wild-type (WT) cells in which thick, continuous F-actin
114 bundles spun the cell length, the *vln* mutant cells showed that fine F-actin filaments were
115 organized in mesh-like networks and F-actin bundles were lessened in the *vln2/3* double mutant
116 or completely absent in the *vln2/3/4* triple mutant (Figure 1A). In addition, we quantified the
117 reduction of actin bundles in *vln* hypocotyl cells using the parameter skewness, a standard
118 metric used in assessing actin filament bundling in which higher fluorescence intensity of the
119 LifeAct-GFP signal in bundled filaments result in a higher skewness value (Higaki, 2017; Higaki
120 et al., 2010). The *vln2/3* and *vln2/3/4* mutants exhibited progressively reduced skewness
121 compared to the WT, indicative of decreased F-actin bundling in the mutant cells (Figure 1B).

122 In WT cells, prominent F-actin cables often are oriented perpendicularly, in parallel to the cell
123 elongation axis, likely underlying the cell elongation phenotype observed in the hypocotyls in the
124 recent report (Li et al., 2025). To further assess the deficient F-actin network in the hypocotyl of
125 the *vln* mutants, we quantified the average angle of F-actin filaments relative to the horizon, with
126 0° being in the transverse direction and 90° being parallel to the growth direction. In epidermal
127 cells of the WT hypocotyl, due to the presence of longitudinal bundles along the growth
128 direction, F-actin were more parallel to the direction of growth, indicated by a higher average
129 angle. In the *vln2/3* and *vln2/3/4* mutant cells, however, the overall angles become shallower,
130 concomitant with the decrease in these long cables and the increasingly abundant appearance
131 of mesh networks of F-actin (Figure 1C).

132

133 **The dynamic and cell-spanning organization of F-actin is maintained in *vln* mutants.**

134 To evaluate the specific contribution of actin bundling to peroxisome motility, ideally, we should
135 conduct the assessment in a system that retains functional albeit unbundled F-actin filaments.
136 To this end, we characterized the F-actin network in the *vln* mutants using stability, coherency,
137 and density as the metrics. Generally, thick F-actin fibers tend to be stable over time, whereas

138 actin filaments in the mesh network are more dynamic (Henty-Ridilla et al., 2013). Because the
139 F-actin mesh network is pronounced in the *vln2/3* and *vln2/3/4* mutants, we tested whether the
140 altered array organization was associated with rapid actin remodeling in these mutants. Images
141 of F-actin were captured at 5-sec intervals, after which pseudo-colored images from different
142 timepoints were merged. Noticeably, while F-actin in WT cells predominantly appeared in white
143 in the merged images, which is indicative of little if any remodeling, the mutant cells showed
144 more dynamic changes in F-actin organization with each timepoint observed in discrete colors
145 (Figure 2A). Further, the white color in the merged images often correlated with thick, long F-
146 actin bundles that are more static than those filaments in the mesh networks in the same WT
147 cells (Figure 2A). In the *vln2/3* and *vln2/3/4* mutant cells, the three distinct colors were more
148 evidently discerned (Figure 2A). Likewise, quantification of this F-actin stability showed that a
149 significantly higher proportion of F-actin in the *vln* mutants underwent remodeling when
150 compared to those of the WT and the *vln2/3/4* cells had significantly fewer F-actin cables than
151 *vln2/3* (Figure 2B). So, our further characterization of the *vln* mutants supported previous
152 conclusions that loss of these three VLN proteins severely impaired F-actin bundling while
153 leaving a diffuse, dynamic mesh network of F-actin.

154 Coherency is a measure of the degree of isotropy of the F-actin distribution, where 0 indicates
155 entirely random orientation and 1 indicates uniform orientation, characteristic of cells enriched
156 with actin cables. F-actin filaments in WT cells are organized in a pattern with higher coherence
157 values compared to more disordered filaments with coherence closer to 0 in the *vln2/3* and
158 *vln2/3/4* mutants (Figure 2C). The decreased coherency in the *vln* mutants suggests dispersed,
159 mesh F-actin, as a consequence of the reduced presence of cell-spanning F-actin bundles.

160 To further characterize the more diffuse, less linear F-actin network in *vln* mutants, we quantified
161 the density of F-actin by measuring the percentage of F-actin occupancy in the cytoplasm. The
162 *vln2/3* cells exhibited significantly higher F-actin occupancy than the WT cells, and the F-actin
163 density in the higher order *vln2/3/4* mutant approximately doubled from that of the WT (Figure
164 2D). The increased F-actin occupancy suggests that the F-actin network, despite being devoid
165 of conspicuous bundles, still spans the cortex, and therefore the cytoskeletal apparatus capable
166 of supporting organelle motility across the whole cell should persist in the mutants.

167 To learn intracellular localization of the VLN proteins, we first had a VLN2-GFP fusion protein
168 expressed under the control of its own promoter in the *vln2/3* double mutant. Because growth
169 phenotype was suppressed by VLN2-GFP expression (Supple. Figure 2A), this fusion protein
170 was functional. When this functional VLN2-GFP was co-expressed with LifeAct-mScarlet-I, the

171 VLN2 was most conspicuously detected on F-actin bundles (Supple. Figure 2B). A mCherry-
172 VLN4 fusion protein also decorated F-actin bundles marked by LifeAct-GFP (Supple. Figure
173 2B).

174 Taken together, our data showed that in the *vln* mutants, F-actin dynamic polymerization and
175 cell-spanning organization is maintained while only cable formation is deficient. As such, these
176 knockout mutants can serve as an informative genetic material to study the role of actin bundles
177 in peroxisome motility.

178

179 **VLN-dependent actin bundling facilitates peroxisome movement**

180 To determine the impact of actin bundling in peroxisome movement and distribution in
181 Arabidopsis, we transformed WT, *vln2/3*, and *vln2/3/4* plants with constructs for the markers of
182 F-actin (LifeAct-GFP) and peroxisome (mScarlet-I-SRL) and visualized them simultaneously in
183 the hypocotyl cells of plants co-expressing the two fusion proteins. The transgenic *vln* double
184 and triple mutants exhibited the progressive deficiencies in F-actin bundling, resembling what
185 was observed earlier in this study. These defects were concomitant with the progressive
186 aggregation of peroxisomes, suggesting an inability of peroxisomes to be distributed uniformly
187 across the cell (Figure 3A). Time-lapse images, taken at 5-sec intervals in epidermal cells of the
188 hypocotyl, revealed that peroxisomes maintained motility along the F-actin tracks in both *vln2/3*
189 double and *vln2/3/4* triple mutants (Figure 3A, Movie S1). Moreover, each track of peroxisome
190 movement was heterogenous, with some rapid movements (>1.5 μm/s) as well as more
191 frequently observed slower movements (<0.5 μm/s), similar to what was observed in the WT
192 (Figure 3B), indicating that the mechanisms of actomyosin-dependent peroxisome movement
193 were at least partially maintained in the *vln* mutants.

194 We first compared the speed of peroxisome movement among the three genotypes of WT,
195 *vln2/3* and *vln2/3/4*. Despite variations in instantaneous speed during imaging duration, the
196 mean speed of each peroxisome movement revealed that only the severe inhibition of F-actin
197 bundling in *vln2/3/*4 caused a significant decrease in the mean speed, while intermediate
198 bundling in *vln2/3* was sufficient to maintain peroxisome speed comparable to that of the WT
199 (Figure 3B). These data suggest that peroxisome movement is facilitated by both discrete F-
200 actin filaments and densely bundled actin cables. To exclude peroxisomes that potentially were
201 unable to associate with F-actin via myosin in the mutants, we calculated the maximum speed
202 of peroxisome movement, defined as the highest instantaneous speed recorded between two

203 consecutive timepoints, to assess the movement of peroxisomes already associated with
204 myosin motors. Again, the maximum speed distributions were not significantly different between
205 WT and *vln2/3*, whereas peroxisome movement was more frequently observed at slower
206 maximum speeds in *vln2/3/4* (Figure 3C). We therefore concluded that the actin dynamics and
207 organization influence peroxisome velocity.

208

209 **Fast, directional peroxisome movement is regulated by F-actin cables**

210 Since the heterogenous patterns of peroxisome motility biased towards slower speeds in the
211 absence of longitudinal actin bundles, as shown in the *vln2/3/4* triple mutants, we hypothesized
212 that F-actin cables specifically facilitate fast, linear movement, which consequently enables
213 uniform peroxisome distribution across the cell. To test this, we evaluated total moving distance,
214 displacement, straight-line speed, overall linearity of movement, and directional change rate
215 (Figure 4A-E). We first measured the total moving distance and found most peroxisomes
216 traversed similar distances with no significant difference among WT, *vln2/3,* and *vln2/3/4* mutant
217 cells (Figure 4A). However, whereas peroxisomes in *vln2/3/4* have a significantly shorter
218 displacement, measured as the shortest distance between the start and end points of the
219 tracked peroxisome (Figure 4B). Furthermore, a consistent phenotype was observed when the
220 displacement distance was normalized by track duration, as represented by “straight-line
221 speed”, which accounted for any differences in the number of motions tracked (Figure 4C).
222 Together these data suggest that, while peroxisomes still move in short bursts that sum to a
223 similar distance observed between *vln* mutants and WT, peroxisomes did not travel as far
224 distance in the *vln2/3/4* mutant in the absence of prominent F-actin bundles or cables when
225 compared to WT or the *vln2/3* mutant. In fact, peroxisomes in *vln2/3/4* mutants shifted direction
226 more frequently than those in the WT cells and their motility was overall less linear and more
227 frequently changed directions (Figure 4D, E), likely because their movement predominantly
228 employed the dynamic F-actin mesh network rather than stable, longitudinal bundles as the
229 tracks.

230 To better assess the heterogenous motility patterns of peroxisomes, we employed a Pearson’s
231 correlation matrix to conduct pairwise analysis of the influence of the aforementioned motility
232 parameters on each other within individual genotypes. While both *vln* mutant genotypes showed
233 correlations comparable to wildtype between average velocity, maximum speed, total distance
234 and track displacement, the correlations between parameters that account for directional

movement (straightforward speed, linearity, and directional change rate) varied across genotypes (Supple. Figure S3A). We then plotted the data of straight-line speed, linearity, and directional change rate from all genotypes in a 3-dimensional scatterplot and used k-means clustering to group motility according to these multidimensional criteria (Figure 5A). The 3 clusters, determined using the Elbow Plot method (Supple. Figure S3B), comprised high straightforward speed and linearity but low directional change rate (Cluster 1); intermediate straightforward speed, linearity, and directional change (Cluster 2); and low straightforward speed and linearity but high directional change rate (Cluster 3). Cluster 1, therefore, was enriched for peroxisomes that rapidly and directionally traversed the cell with minimal turns, while Cluster 3 represented peroxisomes that move in short bursts with frequent changes in direction. Interestingly, WT peroxisomes exhibited uniformly heterogeneous movement, with roughly one third of their tracked movements represented by each of the three clusters (Figure 5B). However, in the vln2/3 mutants, a smaller proportion of peroxisomes move directionally (29.6%), as characterized by Cluster 1, compared to WT (32.8%), and the peroxisome motility profiles shifted towards intermediate (Clusters 2) and short burst (Clusters 3) movements (Figure 5B). In the *vln2/3/4* triple mutant, the reduction in fast, linear peroxisome movements was further exacerbated (20.6%), with more peroxisomes moving in short bursts (39.8%), compared to the WT (30.5%). This shift in cluster populations across genotypes suggests that a lesser proportion of peroxisomes move quickly and linearly when F-actin bundling is deficient in the *vln* mutants.

Taken together, our results showed that densely bundled F-actin cables were necessary for rapid, directional movement of peroxisomes, which enabled the subcellular distribution of peroxisomes required for their diverse metabolic functions.

DISCUSSION

We used the independently generated *vln2/3/4* triple mutant to investigate the synergistic roles of three F-actin bundling VLN proteins in the dynamics and organization of the F-actin network. Our quantitative analysis of peroxisome motility in the WT and *vln* mutants showed that such VLN-dependent F-actin organization is required for rapid directional movement of peroxisomes in the epidermal cells of the Arabidopsis hypocotyls.

266 The plant VLN proteins are grouped into three classes and VLN4 belongs to the class III while
267 VLN2 and VLN3 are in class II (Khurana et al., 2010). Consistent with what was reported
268 recently (Li et al., 2025), the loss of VLN4 greatly enhanced the defects observed in the *vln2/3*
269 double mutant. Therefore, these results collectively indicated that the function of these three
270 VLN proteins, despite being in two different classes, converged towards stabilizing F-actin and
271 promoting high order F-actin bundle formation in vegetative tissues. However, when the three
272 VLN proteins were examined individually without an F-actin marker, they exhibited different
273 extents of F-actin decoration in different tissues (Li et al., 2025). It would be interesting to learn
274 how these proteins localize and function in concert along F-actin filaments *in vivo*. Surprisingly,
275 additional mutations in two other *VLN* genes encoding class I and III VLN proteins did not
276 further enhance the growth phenotypes observed in the *vln2/3/4* triple mutant (Li et al., 2025).
277 Nevertheless, this finding suggested that the three VLN proteins included in our study played
278 the primary role in F-actin bundling.

279 Longitudinally oriented, prominent F-actin cables are found in interphase plant cells and often
280 are considered the primary tracks of long-distance transport of organelles for their robust
281 anisotropic expansion (Garcia-González and van Gelderen, 2021). Here, the *vln2/3/4* triple
282 mutant informed us that fine filaments of F-actin are equally qualified for directional transport of
283 peroxisomes. But the long, stable F-actin bundles exhibited great advantages of promoting
284 rapid, directional movement. Compromises of such rapid, directional movement have a
285 profound consequence in cell expansion.

286 Phenotypic analysis in myosin mutants unequivocally demonstrated that directional movement
287 of organelles like peroxisomes is dependent on Myosin XI motors (Peremyslov et al., 2010;
288 Perico and Sparkes, 2018). It is intriguing how specific organelle would be actively transported
289 with such a wide range of speeds. We hypothesize that the heterogeneity of peroxisome motility
290 is probably brought about by different Myosin XI motors that exhibit different motile activities
291 (Haraguchi et al., 2016). At least 7 of 13 Myosin XI motors in *A. thaliana* had their DIL (dilute)
292 domains that exhibit peroxisome-binding activities when truncations including the domains are
293 ectopically expressed in a heterologous system (Sattarzadeh et al., 2011). However, it is yet to
294 be determined whether the full-length myosin proteins are associated with the organelle when
295 expressed under their native promoters. Alternatively, multiple motors could bind to an organelle
296 to increase the movement processivity and velocity so that it can be transported for long
297 distance, especially in giant cells of organisms like *Chara corallina* (Shimmen and Yokota,
298 2004). Varied numbers of active motors per peroxisome, which is hard to be quantified *in vivo*,

299 likely contribute to the heterogeneity in transport velocities as well. The significance of the
300 heterogeneous peroxisome movement is unclear. Perhaps peroxisome motility may be coupled
301 with the position of other organelles to facilitate inter-organelle communication. So, it would be
302 interesting to determine whether certain patterned movement events were shared by other
303 organelles. Alternatively, peroxisome velocities could vary across the cytoplasm and were
304 coupled with geometrically determined space. In addition, various intrinsic or extrinsic factors
305 cause each peroxisome to display distinct velocities and directionalities.

306

307 **METHODS AND MATERIALS**

308

309 **Plant genotype and growth**

310

311 *Arabidopsis thaliana* plants were grown in soil in a growth chamber at 21°C with cycles of 16hr
312 light and 8hr dark. *Arabidopsis* seedlings that were used for imaging were sterilized and sowed
313 onto ½ Murashige & Skoog Basal media with 0.8% phytagel. Seeds in solid media were cold
314 stratified for 2 days then moved into the growth chamber for 6 days before imaging. All
315 *Arabidopsis thaliana* mutants and wild-type plants are in the Col-0 genetic background. Floral
316 dipping method was used to deliver transgenes into the plant, following established protocols.

317 Mutants of *VLN4* were isolated from seed stock of SALK_109099C (Arabidopsis Biological
318 Resource Center, Ohio State University), which carried a T-DNA insertion in the 12th intron of the
319 *VLN4* gene. The *vln2/3* double mutant was described in an earlier publication (Bao et al., 2012).

320

321 **Plasmid construction**

322

323 To produce an expression vector carrying cassettes for expression of both mScarlet-I-PTS1 and
324 LifeAct-GFP, we first had the codon-optimized mScarlet-I-encoding DNA fragment synthesized
325 commercially (Integrated DNA Technologies, Inc.). The SRL-coding sequence was added to its
326 3' end by PCR using primers of 5'- GTA CCG AAT GGT GAG CAA GGG AGA AG-3' and 5'-CGG
327 CGC GCC TTA TAG CCG GCT TTT ATA CAG TTC GTC CAT ACC GCC G-3'. The fragment

328 was inserted into a plasmid containing the promoter sequence of EF1α (AT1G07920).
329 Separately, the LifeAct-coding sequence was synthesized and inserted into pENTR4 (Thermo
330 Fisher). The resulting plasmid was used to generate a plasmid expressing LifeAct-GFP under
331 the viral 35S promoter by Gateway LR cloning with the pGWB5 plasmid (Nakagawa et al.,
332 2007). The resulting plasmid was linearized by ApaI where the DNA fragment for
333 EF1α(p)::mScarlet-I-PTS1, amplified by the primers of 5'- GCG ACA ATA TGA TCG GGC CTC
334 CGG TGT CAA TCT CAG G-3' and 5'- TGT GGA CGC CGG GCC TTA TAG CCG GCT TTT ATA
335 CAG TTC G-3' from the plasmid described above, was inserted by Gibson reaction to give rise
336 to the plasmid pLB187 used for transformation.

337 To generate the *VLN2* expression plasmid, a 7-kb genomic *VLN2* genomic fragment containing
338 1.1-kb of the predicted promoter region was amplified by using the primers 5'-GAA CCA ATT
339 CAG TCG ACT GGA TCC GGT ACC TCT TTT GAG CTC TAA TTA ATT TTG GAT GAC-3' and
340 5'-TCC AGA GGA TCC AGA TGA ACC AGA AGA ACC GAA CAA GTC GAA CTT CTT CTT AAG
341 CAG-3'. The amplified fragment was introduced into a modified entry vector containing a C-
342 terminus GFP and PA tag (Huang et al., 2024) by Gibson Assembly. The resulting *VLN2* entry
343 plasmid was recombined with the destination vector pGWB1 (Nakagawa et al., 2007) by an LR
344 reaction to produce the *VLN2* expression plasmid.

345 To generate the *VLN4* expression plasmid, a 5-kb *VLN4* genomic CDS fragment was amplified
346 by using the primers 5'-TGT ACA AGG GCG CAG GCG CGA TGT CTG TTT CTA TGA GAG
347 ATT TAG ATC-3' and 5'-TTG TAC AAG AAA GCT GGG TCT AGA TTC AGA AAA GCT GAA CAG
348 CCA TTT TG-3'. The amplified fragment was inserted into a modified entry vector containing an
349 N-terminus mCherry-coding sequence by Gibson Assembly. The resulting plasmid was then
350 linearized by PCR with the primers 5'-TAT GGT GAG CAA GGG CGA GGA G-3' and 5'-CAG
351 TCG ACT GAA TTG GTT CCC ATG G-3'. A 2.5-kb predicted promoter fragment of the *VLN4*
352 gene is amplified by using the primers 5'-GGG AAC CAA TTC AGT CGA CTG ATT TGA GGT
353 ACG AAG CAG ATG-3' and 5'-TCC TCG CCC TTG CTC ACC ATA CTT AAG CAG TCT TTA
354 CCA CTT TCT C-3'. This *VLN4* promoter fragment and the linearized plasmid described above
355 were assembled together by Gibson Assembly. The resulting *VLN4* entry vector was
356 recombined with pGWB1 by LR reaction to produce the *VLN4* expression plasmid.

357 Plasmid were transformed into the agrobacteria strain Gv3101 prior to floral dipping in the WT,
358 *vln2/3* and *vln2/3/4* plants.

359

360 **Confocal microscopy**

361

362 After germination and growth in the chambers, the seedlings were mounted in water for
363 imaging. Live-cell imaging was performed on an LSM980 laser scanning confocal microscope
364 with the Airyscan2 function using a 40X water immersion objective (Carl Zeiss). Single frame
365 images of F-actin were used to measure orientation, coherency, density and skewness. For
366 measurements of F-actin stability, time-lapse images with 5sec/frame were obtained. Similarly,
367 to image peroxisome movement, both markers for F-actin and peroxisomes were
368 simultaneously imaged with a time-lapsed of 5sec/frame. At least 3 independent transformant
369 lines were imaged per genotype.

370

371 **Quantification of F-actin**

372

373 Images were first rotated such that the direction of growth in along the vertical axis. The images
374 were thresholded, binarized and skeletonized for quantifying F-actin (Higaki, 2017). A region of
375 interest was drawn to select only the cell of interest. The imageJ plugin OrientationJ was used
376 to measure orientation, and coherency (Püspöki et al., 2016). Skewness and density were
377 measured by using the LPX plugin package (Higaki et al., 2010; Schneider et al., 2012).

378 To measure percentage of stable F-actin, we imaged F-actin for 10 seconds at 5 sec/frame. The
379 first and last frames were merged. The assumption is that stable filaments should still be
380 present or unchanged in position after 10 seconds. A stable filament from the last frame should
381 colocalize with a filament from the first frame. The merged image was thresholded for
382 colocalized filaments. The percentage of stable F-actin was calculated using a ratio of
383 colocalized F-actin signal to total F-actin signal.

384

385 **Quantification of peroxisome motility**

386

387 Quantitative measurement of F-actin-dependent peroxisome motility was carried out by imaging
388 both F-actin and peroxisomes simultaneously with 5-sec intervals. Peroxisomes that were

unattached from F-actin were not measured. Peroxisomes were tracked using the ImageJ plugin, TrackMate (Ershov et al., 2022). Previous reports have mentioned that slow moving peroxisomes are usually at least 0.2 μm/sec (Mathur et al., 2002). we excluded peroxisomes that were moving at velocities below 0.1 μm/sec as those appear to be more likely due to Brownian movements. We manually reevaluated the tracks with velocities below 0.1 μm/sec to confirm that these movements appeared oscillatory. The output track data summarized the overall movement of individual peroxisome during the imaging duration, and provided the track features regarding: (1) mean speed for the average speed values over every 5-second intervals along a track; (2) max speed for the highest instantaneous speed between two consecutive timepoints along a track; (3) straight-line speed, for track displacement divided by track duration; (4) total distance traveled; (5) track displacement; (6) linearity of forward progression for the ratio between straight-line speed and track mean speed, when tracks that are completely linear would have a value of 1; and (7) directional change rate for the average angle between consecutive timepoints along a track divided by the track duration.

Acknowledgements

We thank Dr. Shanjin Huang for providing the vln2/3 mutant seeds and Dr. Tsuyoshi Nakagawa for sharing the pGWB plasmids. We also thank Dr. Felicia L. Peng and Dr. Chenxin Li for their advice and comments on this work, and Dr. Thomas Wilkop for his superb microscopic support.

Competing interests

The authors declare no other competing or financial interests.

Author contributions

Conceptualization: C.H.H., Y.-R.J.L., J.H., B.L.; Methodology: C.H.H., A.M.K., Y.-R.J.L., J.H., B.L.; Investigation: C.H.H., Y.-R.J.L.; Formal analysis: C.H.H., A.M.K., Y.-R.J.L.; Visualization: C.H.H., Y.-R.J.L.; Data curation: C.H.H.; Supervision: B.L., J.H.; Project administration: B.L.; Funding acquisition: J.H., B.L.; Writing (original draft): C.H.H., A.M.K.; Writing (review and editing): C.H.H., A.M.K., Y.-R.J.L., J.H., B.L.

Funding

This work was supported by grants from the National Science Foundation (2148206 & 2148207). B.L. was sponsored by the U.S. Department of Agriculture (USDA)-the National Institute of Food and Agriculture (NIFA) under an Agricultural Experiment Station (AES) hatch project (CA-D-PLB-2536-H).

Data and resource availability

All data acquired from this study are included within the main text and Supplementary information.

428 **FIGURE LEGENDS**

429

430 **Figure 1.** The *vln4* mutation enhances the phenotype of F-actin organization caused by the *vln2*
431 and *vln3* mutations in Arabidopsis. (A) F-actin, labeled by the LifeAct-GFP fusion in transgenic
432 wild-type (WT), *vln2/3*, *vln2/3/4* plants, is imaged at the cell cortex of hypocotyl epidermal cells.
433 The WT cell has cortical F-actin in two populations of long, thick bundles and finer filaments in
434 mesh network. The prominent bundles are reduced in the *vln2/3* double mutant and almost
435 completely lost in the *vln2/3/4* triple mutant. Maximum projections of the LifeAct-GFP images
436 are shown. (B) The skewness of the F-actin is measured to reflect how well the filaments are
437 bundled. Values were measured from n>35 cells of each genotype. (C) Quantitative assessment
438 of F-actin orientation. The orientation is determined with a 90° angle perpendicular to cell
439 elongation axis. Significance is determined by a two-tailed t-test with $p < 0.01$ (****). Scale bar: 5
440 μm.

441

442 **Figure 2.** Effects of *vln* mutations on the dynamics of F-actin in Arabidopsis. (A) Three time-
443 lapse images of F-actin are taken at 5-second intervals in the WT, *vln2/3*, and *vln2/3/4* cells.
444 Each frame is pseudo-colored and merged to reflect the changes of F-actin filaments. Stable
445 filaments that experience no changes after 10 seconds appear in white in the merged images.
446 WT cells appear to have more of these stable filaments. The double mutant *vln2/3* has fewer
447 stable filaments and the triple mutant *vln2/3/4* mostly has rapidly remodeling F-actin filaments.
448 (B) Quantification of the amount of stable F-actin shows that WT has the highest amount while
449 the *vln2/3* and *vln2/3/4* mutants progressively have fewer. Values are measured from n>35 cells
450 of each genotype. (C) Coherency of F-actin filaments is measured to determine how F-actin
451 filaments are aligned. Higher coherency values represent more ordered filaments in a preferred
452 a specific direction. (D) Comparison of F-actin density in WT, *vln2/3*, and *vln2/3/4* cells. The
453 density value is determined by the proportion (%) of the cell cortex occupied by F-actin.
454 Significance is determined by a two-tailed t-test with $p < 0.01$ (****). Scale bar: 5 μm.

455

456 **Figure 3.** Peroxisome motility is affected in the *vln2/3/4* mutant lacking F-actin bundling. (A)
457 Peroxisome and F-actin are simultaneously imaged with 5-seconds intervals. In the *vln2/3* and
458 *vln2/3/4* mutant cells that have reduced long F-actin bundles, peroxisomes show reduced linear
459 movement. (B-C) Quantitative assessments of average peroxisome speed and maximum speed
460 in WT and *vln* mutants. Values are measured from n>300 peroxisome tracks from each
461 genotype and plotted along a raincloud plot with a histogram on top and a boxplot below. Yellow
462 diamonds represent the mean position. Significance is determined by a Wilcoxon rank sum test
463 with p-values shown in the figures.

464

465 **Figure 4**. Quantitative comparisons of peroxisome tracks in the WT, *vln2/3* and *vln2/3/4* mutant
466 cells. (A-E) Parameters include total distance, track displacement, average straight-line speed,

467 linearity, and directional change rate. Values are measured from n>300 peroxisome tracks from
468 each genotype and plotted along a raincloud plot with a histogram on top and a boxplot below.
469 Yellow diamonds represent the mean values. Significance is determined by a Wilcoxon rank
470 sum test with p-values shown in the figures.

471

472 **Figure 5.** Pairwise correlation analysis of peroxisome movement in terms of directional change
473 rate, average straightforward speed, and linearity. (A) Formation of three clusters following the
474 pairwise correlation analysis. (B) Relative proportions of peroxisome movement in the three
475 clusters in the WT, *vln2/3*, and *vln2/3/4* cells.

REFERENCES

Avisar, D., Prokhnevsky, A. I., Makarova, K. S., Koonin, E. V. and Dolja, V. V. (2008). Myosin XI-K Is required for rapid trafficking of Golgi stacks, peroxisomes, and mitochondria in leaf cells of Nicotiana benthamiana. *Plant Physiol* **146**, 1098-108.

Bao, C. C., Wang, J., Zhang, R. H., Zhang, B. C., Zhang, H., Zhou, Y. H. and Huang, S. J. (2012). Arabidopsis VILLIN2 and VILLIN3 act redundantly in sclerenchyma development via bundling of actin filaments. *Plant Journal* **71**, 962-975.

Covill-Cooke, C., Toncheva, V. S. and Kittler, J. T. (2021). Regulation of peroxisomal trafficking and distribution. *Cellular And Molecular Life Sciences* **78**, 1929-1941.

Ershov, D., Phan, M.-S., Pylvänäinen, J. W., Rigaud, S. U., Le Blanc, L., Charles-Orszag, A., Conway, J. R. W., Laine, R. F., Roy, N. H., Bonazzi, D. et al. (2022). TrackMate 7: integrating state-of-the-art segmentation algorithms into tracking pipelines. *Nature Methods* **19**, 829-832.

Garcia-González, J. and van Gelderen, K. (2021). Bundling up the Role of the Actin Cytoskeleton in Primary Root Growth. *Front Plant Sci* **12**.

Haraguchi, T., Tominaga, M., Nakano, A., Yamamoto, K. and Ito, K. (2016). Myosin XI-I is Mechanically and Enzymatically Unique Among Class-XI Myosins in Arabidopsis. *Plant Cell Physiol* **57**, 1732-43.

He, A. Y., Dean, J. M. and Lodhi, I. J. (2021). Peroxisomes as cellular adaptors to metabolic and environmental stress. *Trends in Cell Biology* **31**, 656-670.

Henty-Ridilla, J. L., Li, J. J., Blanchoin, L. and Staiger, C. J. (2013). Actin dynamics in the cortical array of plant cells. *Current Opinion in Plant Biology* **16**, 678-687.

Higaki, T. (2017). Quantitative evaluation of cytoskeletal organizations by microscopic image analysis. *PLANT MORPHOLOGY* **29**, 15-21.

Higaki, T., Kutsuna, N., Sano, T., Kondo, N. and Hasezawa, S. (2010). Quantification and cluster analysis of actin cytoskeletal structures in plant cells: role of actin bundling in stomatal movement during diurnal cycles in Arabidopsis guard cells. *Plant Journal* **61**, 156-165.

Huang, C. H., Peng, F. L., Lee, Y. R. J. and Liu, B. (2024). The microtubular preprophase band recruits Myosin XI to the cortical division site to guide phragmoplast expansion during plant cytokinesis. *Developmental Cell* **59**, 2333-2346.e6.

Huang, S., Qu, X. and Zhang, R. (2015). Plant villins: versatile actin regulatory proteins. *J Integr Plant Biol* **57**, 40-9.

Khurana, P., Henty, J. L., Huang, S. J., Staiger, A. M., Blanchoin, L. and Staiger, C. J. (2010). VILLIN1 and VILLIN3 Have Overlapping and Distinct Activities in Actin Bundle Formation and Turnover. *Plant Cell* **22**, 2727-2748.

Koenig, A. M., Liu, B. and Hu, J. P. (2023). Visualizing the dynamics of plant energy organelles. *Biochemical Society Transactions* **51**, 2029-2040.

Li, X., Zhuang, Y. H., Zhao, W. Y., Qu, X. L., Wang, J., Chang, M., Shen, J. F., Chen, N. Z. and Huang, S. J. (2025). Molecular and functional adaption of Arabidopsis villins. *New Phytologist* **245**, 1158-1179.

Mathur, J., Mathur, N. and Hulskamp, M. (2002). Simultaneous visualization of peroxisomes and cytoskeletal elements reveals actin and not microtubule-based peroxisome motility in plants. *Plant Physiol* **128**, 1031-45.

Nakagawa, T., Kurose, T., Hino, T., Tanaka, K., Kawamukai, M., Niwa, Y., Toyooka, K., Matsuoka, K., Jinbo, T. and Kimura, T. (2007). Development of series of gateway binary vectors, pGWBs, for realizing efficient construction of fusion genes for plant transformation. *J Biosci Bioeng* **104**, 34-41.

Neuhaus, A., Eggeling, C., Erdmann, R. and Schliebs, W. (2016). Why do peroxisomes associate with the cytoskeleton? *Biochimica Et Biophysica Acta-Molecular Cell Research* **1863**, 1019-1026.

Pan, R. H., Liu, J., Wang, S. S. and Hu, J. P. (2020). Peroxisomes: versatile organelles with diverse roles in plants. *New Phytologist* **225**, 1410-1427.

Peremyslov, V. V., Prokhnevsky, A. I. and Dolja, V. V. (2010). Class XI myosins are required for development, cell expansion, and F-Actin organization in Arabidopsis. *Plant Cell* **22**, 1883-97.

Perico, C. and Sparkes, I. (2018). Plant organelle dynamics: cytoskeletal control and membrane contact sites. *New Phytologist* **220**, 381-394.

Püspöki, Z., Storath, M., Sage, D. and Unser, M. (2016). Transforms and Operators for Directional Bioimage Analysis: A Survey. *Focus on Bio-Image Informatics* **219**, 69-93.

Salogiannis, J. and Reck-Peterson, S. L. (2017). Hitchhiking: A Non-Canonical Mode of Microtubule-Based Transport. *Trends in Cell Biology* **27**, 141-150.

Sandalio, L. M., Peláez-Vico, M. A., Molina-Moya, E. and Romero-Puertas, M. C. (2021). Peroxisomes as redox-signaling nodes in intracellular communication and stress responses. *Plant Physiology* **186**, 22-35.

Sattarzadeh, A., Schmelzer, E. and Hanson, M. R. (2011). Analysis of Organelle Targeting by DIL Domains of the Arabidopsis Myosin XI Family. *Front Plant Sci* **2**, 72.

Schneider, C. A., Rasband, W. S. and Eliceiri, K. W. (2012). NIH Image to ImageJ: 25 years of image analysis. *Nat Methods* **9**, 671-675.

Shimmen, T. and Yokota, E. (2004). Cytoplasmic streaming in plants. *Curr Opin Cell Biol*. **16**, 68-72.

van der Honing, H. S., Kieft, H., Emons, A. M. C. and Ketelaar, T. (2012). Arabidopsis VILLIN2 and VILLIN3 Are Required for the Generation of Thick Actin Filament Bundles and for Directional Organ Growth. *Plant Physiology* **158**, 1426-1438.

Wanders, R. J. A., Baes, M., Ribeiro, D., Ferdinandusse, S. and Waterham, H. R. (2023). The physiological functions of human peroxisomes. *Physiol Rev* **103**, 957-1024.

Yokota, E., Vidali, L., Tominaga, M., Tahara, H., Orii, H., Morizane, Y., Hepler, P. K. and Shimmen, T. (2003). Plant 115-kDa actin-filament bundling protein, P-115-ABP, is a homologue of plant villin and is widely distributed in cells. *Plant and Cell Physiology* **44**, 1088-1099.

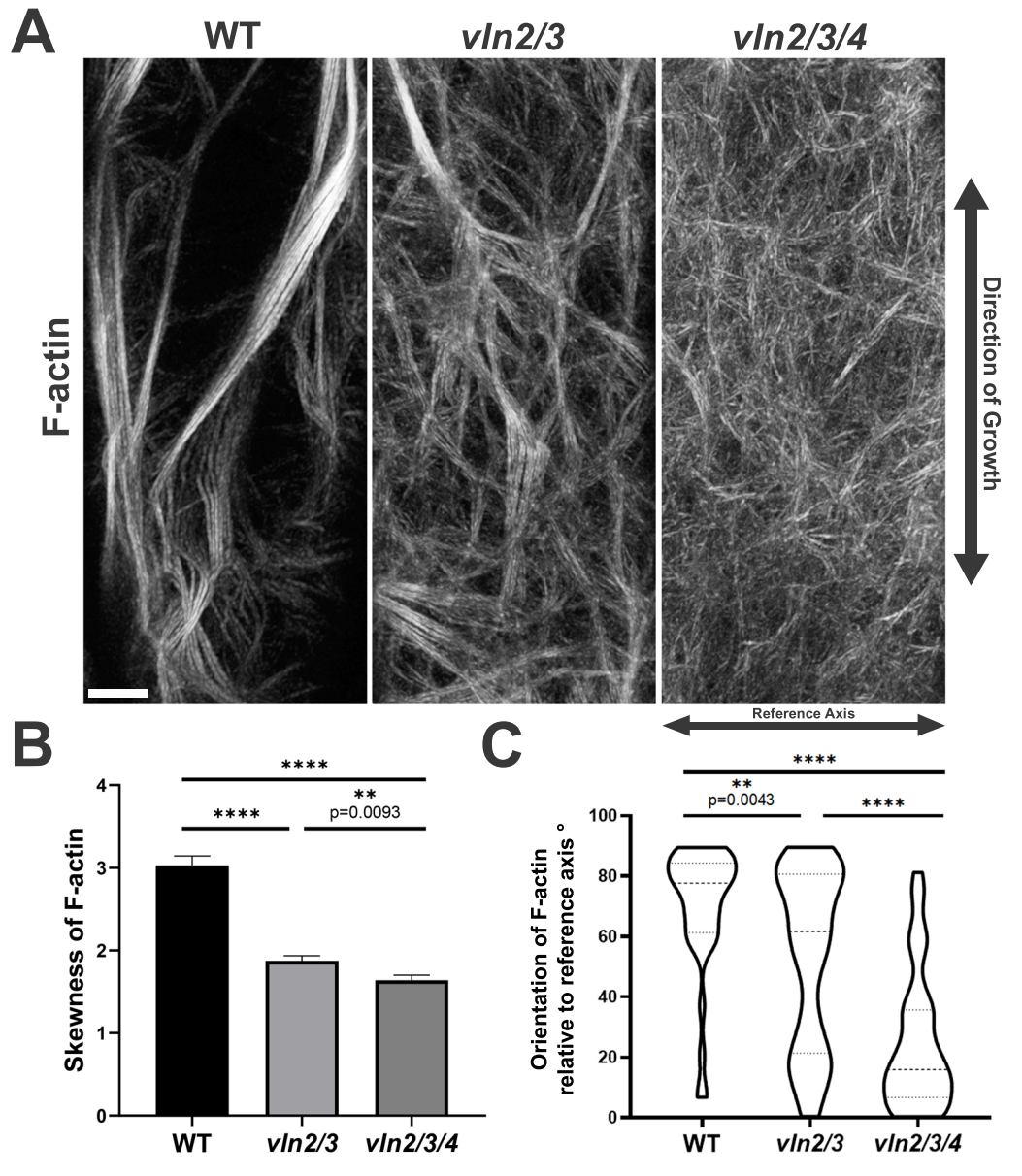
A
WT
vln2/3
vln2/3/4
F-actin
Direction of Growth
Reference Axis
B
Skewness of F-actin
****
**
p=0.0093
****
0
1
2
3
4
WT
vln2/3
vln2/3/4
C
Orientation of F-actin relative to reference axis °
****
**
p=0.0043
****
0
20
40
60
80
100
WT
vln2/3
vln2/3/4

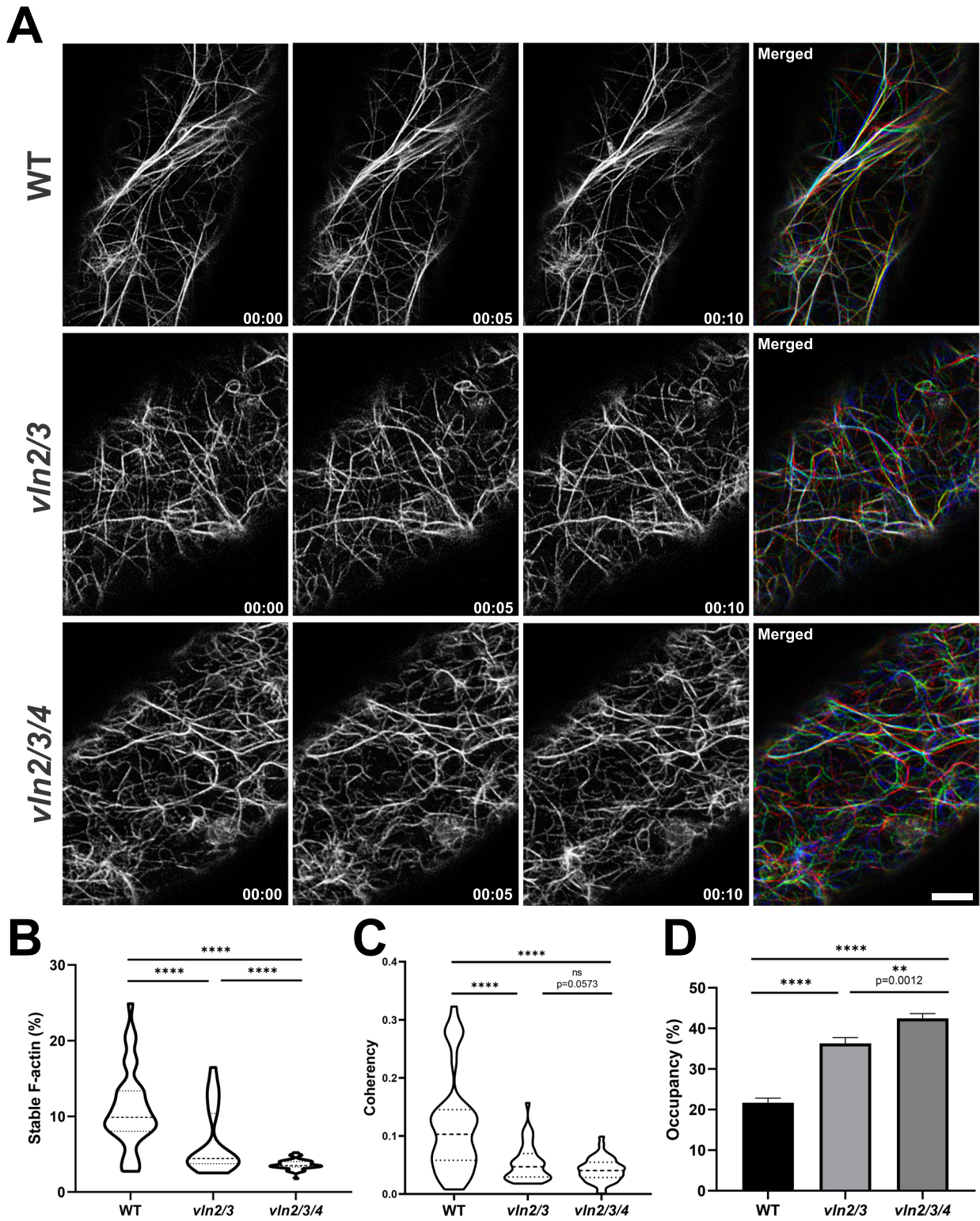
A
WT
vln2/3
vln2/3/4
Merged
00:00
00:05
00:10
B
Stable F-actin (%)
30
20
10
0
****
****
****
WT
vln2/3
vln2/3/4
C
Coherency
0.4
0.3
0.2
0.1
0.0
****
****
ns
p=0.0573
WT
vln2/3
vln2/3/4
D
Occupancy (%)
50
40
30
20
10
0
****
****
**
p=0.0012
WT
vln2/3
vln2/3/4

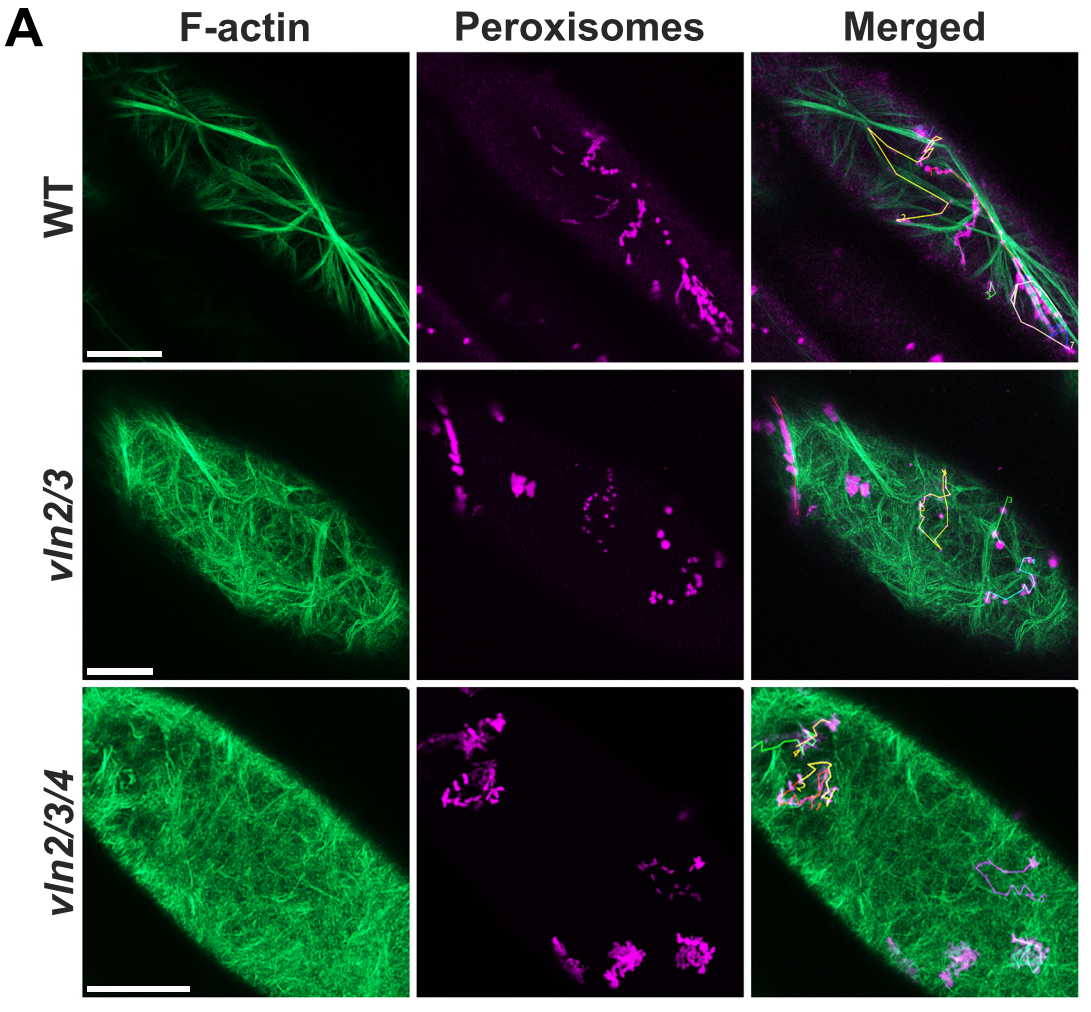
A
F-actin
Peroxisomes
Merged
WT
vln2/3
vln2/3/4

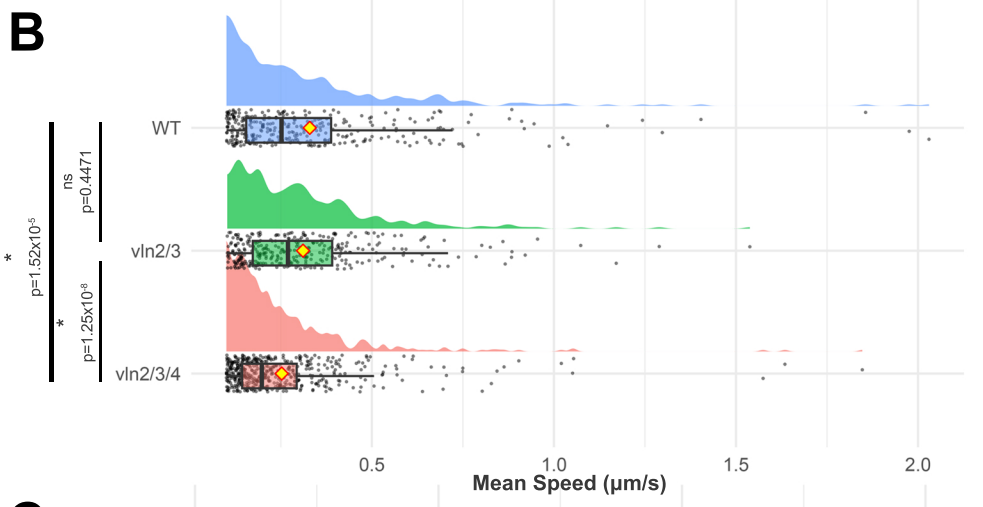
B
WT
vln2/3
vln2/3/4
ns
p=0.4471
*
p=1.52x10-5
*
p=1.25x10-8
0.5
1.0
1.5
2.0
Mean Speed (µm/s)

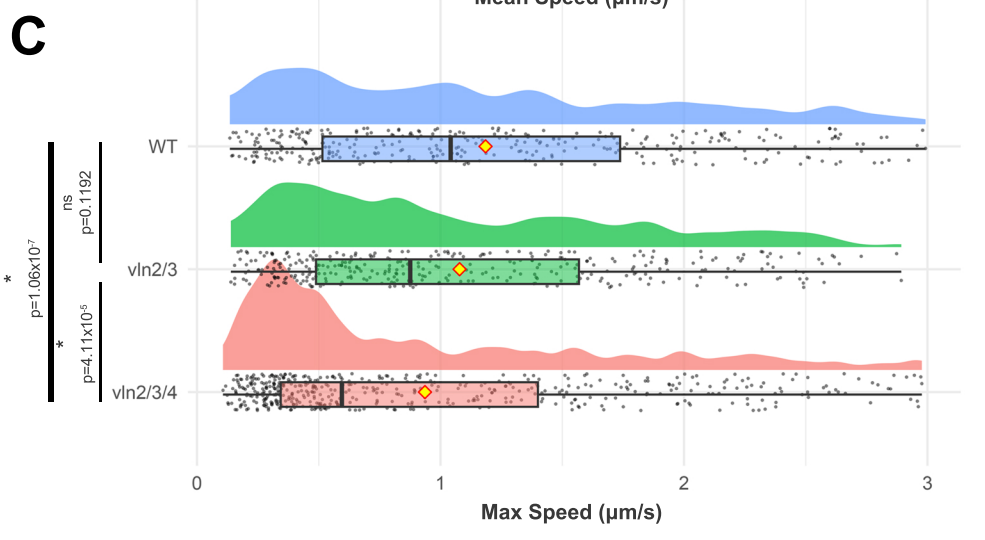
C
WT
vln2/3
vln2/3/4
ns
p=0.1192
*
p=1.06x10-7
*
p=4.11x10-5
0
1
2
3
Max Speed (µm/s)

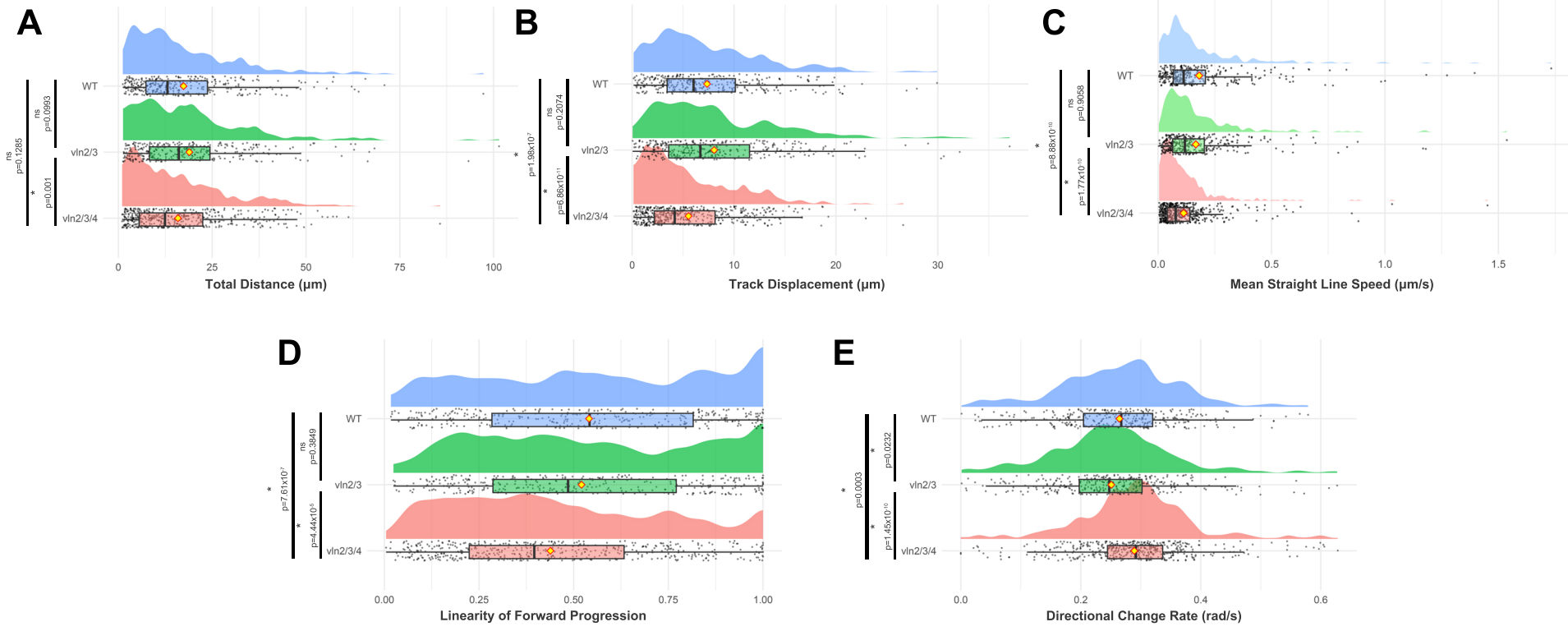
A
WT
vln2/3
vln2/3/4
ns
p=0.1285
ns
p=0.0923
*
p=0.001
0
25
50
75
100
Total Distance (µm)
B
WT
vln2/3
vln2/3/4
ns
p=0.2074
*
p=1.98x10^-7
*
p=6.86x10^-11
0
10
20
30
Track Displacement (µm)
C
WT
vln2/3
vln2/3/4
ns
p=0.28358
*
p=8.86x10^-10
*
p=1.77x10^-10
0.0
0.5
1.0
1.5
Mean Straight Line Speed (µm/s)
D
WT
vln2/3
vln2/3/4
*
p=7.61x10^-7
ns
p=0.3849
*
p=4.44x10^-6
0.00
0.25
0.50
0.75
1.00
Linearity of Forward Progression
E
WT
vln2/3
vln2/3/4
*
p=0.0003
*
p=0.0232
*
p=1.45x10^-6
0.0
0.2
0.4
0.6
Directional Change Rate (rad/s)

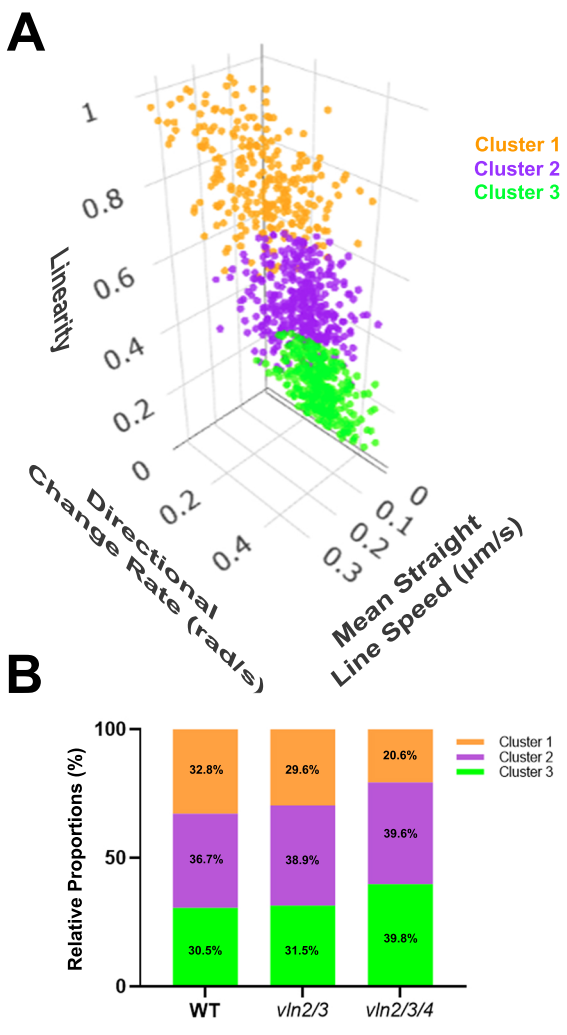
A
Cluster 1
Cluster 2
Cluster 3
Linearity
1
0.8
0.6
0.4
0.2
0
Directional Change Rate (rad/s)
0.2
0.4
Mean Straight Line Speed (μm/s)
0
0.1
0.2
0.3
B
Relative Proportions (%)
100
50
0
32.8%
36.7%
30.5%
29.6%
38.9%
31.5%
20.6%
39.6%
39.8%
WT
vln2/3
vln2/3/4
Cluster 1
Cluster 2
Cluster 3